GDCh Research Article Angewandte International Edition Chemie www.angewandte.org

How to cite: *Angew. Chem. Int. Ed.* **2024**, e202410043
doi.org/10.1002/anie.202410043

MOF Membranes

Crystalline Metal–Organic Framework Coatings Engineered via Metal–Phenolic Network Interfaces

*Tianzheng Wang, Zhixing Lin, Omid Mazaheri, Jingqu Chen, Wanjun Xu, Shuaijun Pan, Chan-Jin Kim, Jiajing Zhou, Joseph J. Richardson, and Frank Caruso**

Abstract: Crystalline metal–organic frameworks (MOFs) have garnered extensive attention owing to their highly ordered porous structure and physicochemical properties. However, their practical application often requires their integration with various substrates, which is challenging because of their weakly adhesive nature and the diversity of substrates that exhibit different properties. Herein, we report the use of amorphous metal–phenolic network coatings to facilitate the growth of crystalline MOF coatings on various particle and planar substrates. Crystalline MOFs with different metal ions and morphologies were successfully deposited on substrates (13 types) of varying sizes, shapes, and surface chemistries. Furthermore, the physicochemical properties of the coated crystalline MOFs (e.g., composition, thickness) could be tuned using different synthesis conditions. The engineered MOF-coated membranes demonstrated excellent liquid and gas separation performance, exhibiting a high H_2 permeance of 63200 GPU and a H_2/CH_4 selectivity of 10.19, likely attributable to the thin nature of the coating (~180 nm). Considering the vast array of MOFs available (>90,000) and the diversity of substrates, this work is expected to pave the way for creating a wide range of MOF composites and coatings with potential applications in diverse fields.

[*] T. Wang, Dr. Z. Lin, Dr. O. Mazaheri, Dr. J. Chen, Dr. W. Xu, Prof. S. Pan, Dr. C.-J. Kim, Prof. J. Zhou, Dr. J. J. Richardson, Prof. F. Caruso
Department of Chemical Engineering
The University of Melbourne
Parkville, Victoria 3010, Australia
E-mail: fcaruso@unimelb.edu.au

Dr. J. J. Richardson
School of Engineering
RMIT University
Melbourne, Victoria 3000, Australia

Introduction

Surface engineering strategies and thin-film coatings are fundamentally important in designing advanced materials for diverse applications as they afford control over interfaces. Crystalline metal–organic frameworks (MOFs) (coordination polymers of metal ions and organic ligands) have received significant scientific and industrial attention owing to their high surface areas, well-defined porous structures, and hybrid physicochemical properties originating from the metal ions and organic ligands, leading to the discovery of over 90000 distinct MOFs.[1–3] However, for practical usage, MOFs often need to be integrated with different devices and surfaces. In particular, MOF coatings on particle and planar substrates endow composites with desired functionalities in various fields,[4] including catalysis,[5,6] biomedicine,[7–9] energy,[10] and environmental applications.[11–13] To facilitate the formation of crystalline MOF coatings on different substrates, various strategies have been employed, including microwave-assisted synthesis,[14] seeded growth,[15,16] counter-diffusion growth,[17,18] and solvent-free conversion.[19–21] However, these strategies are often only applicable to a substrate type, are time-consuming, and/or require specialized and/or harsh experimental conditions (e.g., high temperature or pressure) owing to the relatively low affinity of crystalline MOFs for most substrates.[6,14–23] Alternatively, surface modification of the substrates prior to MOF formation can be conducted, which is simple and does not necessitate significant alterations to the well-developed synthesis protocols of different MOFs.[6,24–28] However, a tailored modification strategy is generally required specific to the distinct physicochemical properties of the substrates and MOFs (e.g., composition, size, surface charge, and morphology).[25,26,28] Thus, there is a need for a simple and universal surface modification approach amenable to the different synthesis conditions and solvents common to MOF crystallization and amenable to the diverse substrates required for the application of crystalline MOFs.

Polyphenols are natural phenolic molecules that can bind to various substrates through various interactions, including hydrogen bonding, metal chelation, electrostatics, and hydrophobic interactions.[29] These diverse molecular interactions allow polyphenols to simultaneously coordinate with various metal ions and interact with surfaces to form amorphous coordination network coatings, termed metal–phenolic networks (MPNs), on a wide range of substrates within seconds.[30] Importantly, MPNs retain the inherent ability of the polyphenols to interact with macromolecules

and metals and are stable in a wide range of solvents,[30] making them promising candidates for modifying substrates for the growth of crystalline MOFs on substrates.

Herein, we report a versatile MPN-mediated interfacial engineering strategy to facilitate the growth of crystalline MOF coatings on a wide range of substrates (13 types, Scheme 1, Table S1). An ultrathin MPN coating is first assembled on the substrate in aqueous media at room temperature to provide chelation sites and anchoring for the subsequent growth and crystallization of different MOFs. Various zeolitic imidazolate frameworks (ZIFs), a well-studied class of crystalline MOFs,[31] are chosen as models to demonstrate the feasibility of this strategy, where continuous and thin crystalline MOF films with customized physicochemical properties and crystallinity are engineered. Furthermore, the MOF coatings exhibit excellent liquid and gas separation properties, which is likely attributable to the thin nature of the crystalline MOF coatings (~180 nm). This work provides a strategy to facilitate the formation of crystalline MOF coatings and contributes towards building a materials library of MOF composites with potential in various fields.

Results and Discussion

Interfacial MOF assembly was initiated by first depositing MPNs on substrates under mild conditions (e.g., aqueous solution and room temperature), where the MPN layers then acted as active coordination sites to facilitate the growth and crystallization of MOFs. Here, tannic acid (TA), a natural polyphenol with numerous chelation sites, was selected as the model ligand, and Fe^{3+} was chosen to cross-link the phenolic ligands using a well-established protocol to form stable MPN coatings on polystyrene (PS) particles (diameter: 3.35 μm).[30] The PS suspension changed from white to purple upon the addition of TA and Fe^{3+}, and the surface of the PS particles became rougher, as observed under scanning electron microscopy (SEM), indicating the successful formation of an MPN coating on the PS particles (PS@MPN; Figure 1a, Figure S1a). The MPN coating was further confirmed by visualization of collapsed MPN capsules in the air-dried state upon removal of the PS templates with tetrahydrofuran (Figure 1b, Figure S1b). Subsequently, ZIF-8 precursors, i.e., zinc nitrate hexahydrate ($Zn(NO_3)_2 \cdot 6H_2O$) and 2-methylimidazole (2-MIM), were successively added to the PS@MPN particle suspension to construct crystalline MOF coatings on the MPN-coated PS particles at room temperature (PS@MPN@ZIF-8). The suspension turned white, and nanosized crystals were observed on the particle surface (Figure S1c). In contrast to MPN capsules, removal of the PS templates resulted in self-standing hollow MPN@ZIF-8 capsules that did not collapse after air drying (Figure 1c, Figure S1d), likely due to the presence of continuous and crystalline MOF coatings (~250 nm, Figure S2). Furthermore, changing the synthesis conditions by altering the concentration of the MOF precursors or the metal-to-ligand ratio afforded control over

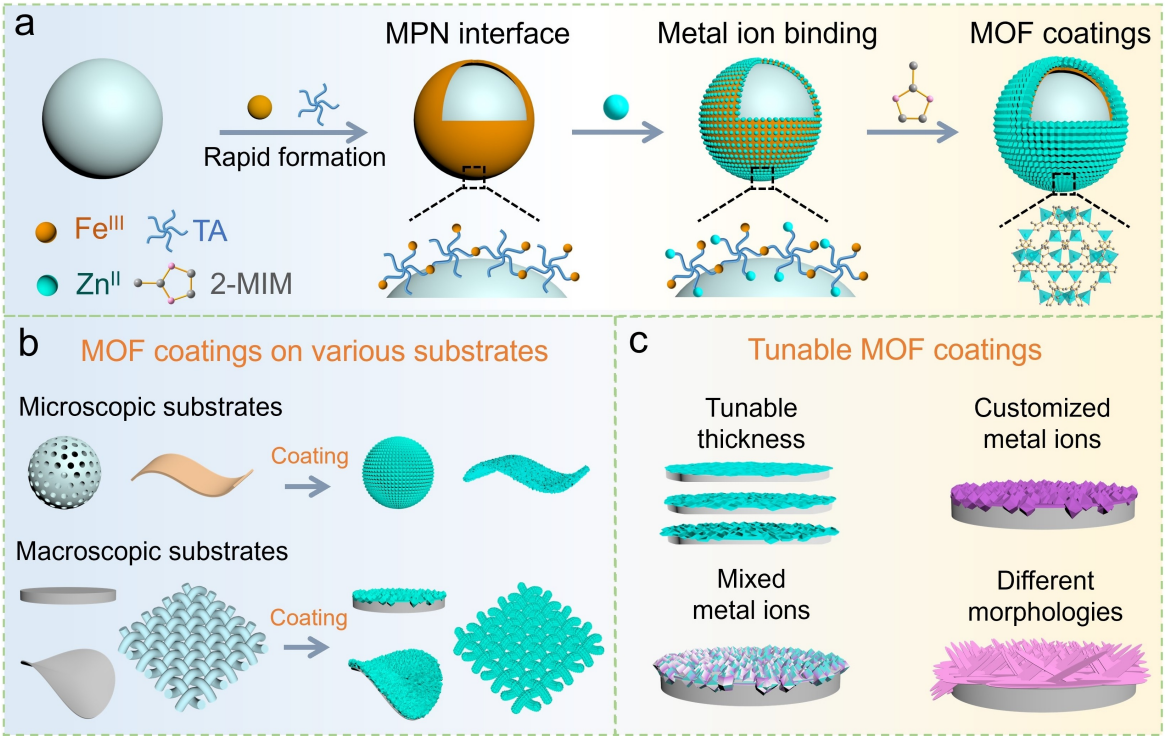

Scheme 1. Schematic illustration of the MPN-mediated growth of crystalline MOFs. (a) Formation and growth of crystalline MOFs (e.g., ZIF-8) on the surface of a particle using MPNs. (b) Applicability of the present strategy to different microscopic (~0.05–5 μm) and macroscopic (~0.5–10 cm) substrates. (c) Properties of MOF coatings that can be tuned using the present strategy.

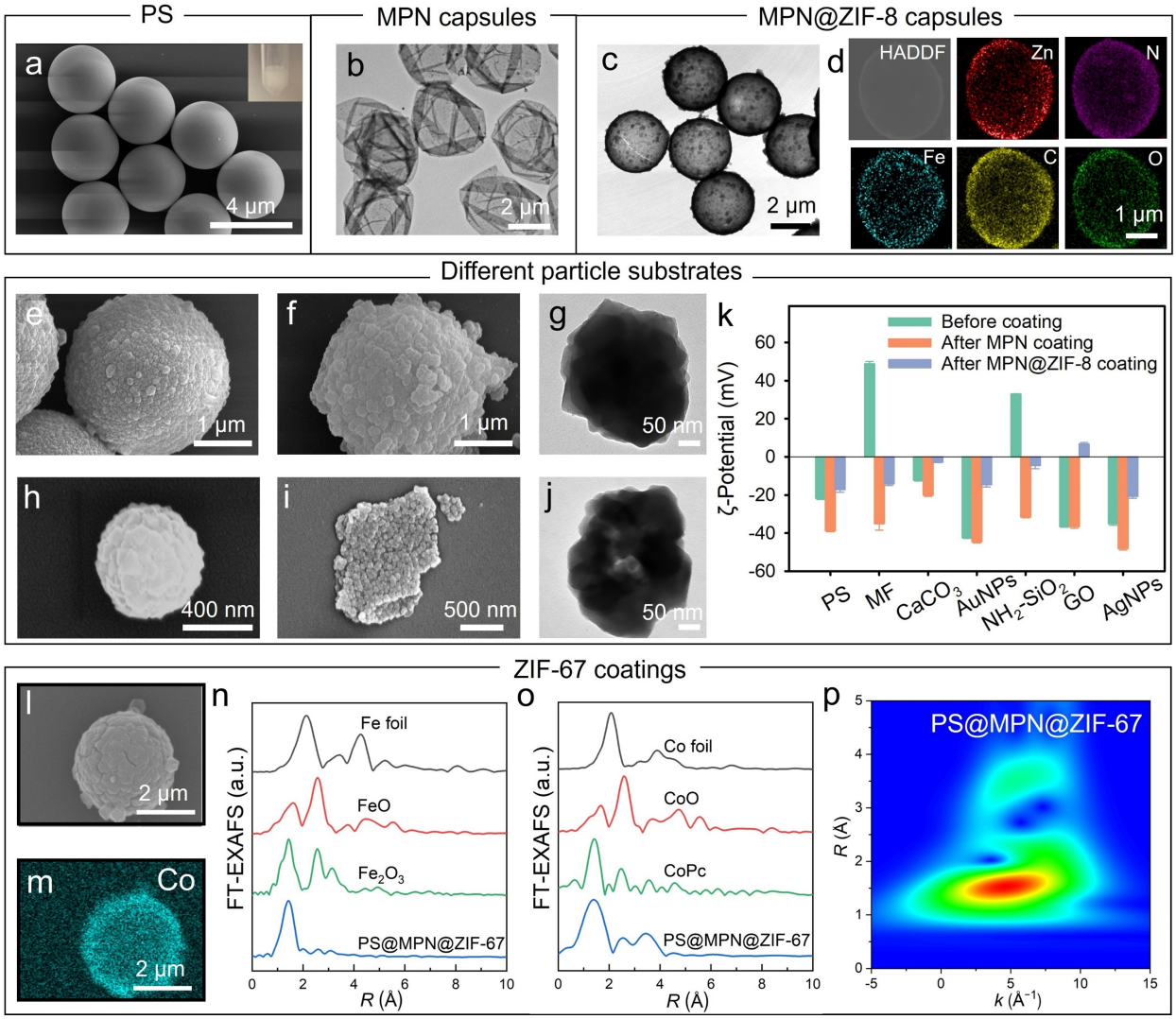

Figure 1. (a) SEM image of PS particles. Inset is the corresponding photograph of a PS particle suspension. (b) TEM image of MPN capsules. (c,d) TEM, HADDF, and EDX images of MPN@ZIF-8 capsules. (e–j) SEM and TEM images of crystalline MOF coatings on diverse MPN-modified substrates, including melamine formaldehyde (MF) (e), $CaCO_3$ (f), gold nanoparticles (AuNPs) (g), aminated SiO_2 (NH_2-SiO_2) (h), graphene oxide (GO) (i), and silver nanoparticles (AgNPs) (j). (k) ζ-Potential values of diverse substrates before and after MPN coating and crystalline MOF coating. The error bars represent standard deviations ($n=3$). ZIF-8 coating in (c–k) was prepared using a Zn^{2+} concentration of 2.86 mg mL^{-1} and a Zn^{2+}-to-2-MIM molar ratio of 1 : 2. (l) SEM image and (m) EDX mapping of ZIF-67 coating after MPN deposition. (n) K-edge FT-EXAFS spectra of iron in Fe foil, FeO, Fe_2O_3, and PS@MPN@ZIF-67. (o) K-edge FT-EXAFS spectra of cobalt in Co foil, CoO, cobalt phthalocyanine (CoPc), and PS@MPN@ZIF-67. (p) WT analysis of PS@MPN@ZIF-67.

the stiffness of the MOF shell, as indicated by their collapsed or self-standing structure, as observed by SEM (Figures S3 and S4). High-angle annular dark-field (HAADF) image and energy-dispersive X-ray spectroscopy (EDX) mapping images confirmed the hollow spherical structure and the presence of Zn and N (attributed to the ZIF-8 coating) as well as Fe (attributed to the MPN coating) on the particle surface (Figure 1d). The ζ-potential of the PS particles shifted from -22 ± 1 to -39 ± 1 mV after MPN coating due to the deprotonation of TA (Figure 1k)[30] and then slightly increased to -17 ± 1 mV after the formation of a subsequent ZIF-8 coating. Furthermore, dynamic light scattering results showed a slightly increased diameter after ZIF-8 coating (Figure S5). Importantly, as observed from Figure S6a, the MPN- and ZIF-8-coated PS particles, i.e., PS@MPN@ZIF-8, exhibited distinct X-ray diffraction (XRD) patterns originating from ZIF-8, indicating the formation of a crystalline structure on the surface. Fourier transform infrared (FTIR) spectra demonstrated distinct peaks at 420 cm^{-1} (Zn–N stretching vibration), 1146 and 1311 cm^{-1} (C–N stretching vibration from in-plane imidazole ring) for the PS@MPN@ZIF-8 particles, which were absent for the PS and PS@MPN samples, further demonstrating the formation of ZIF-8 on the surface of PS@MPN (Figure S6b).[19,32] A comparison study with growing ZIF-8 onto pristine PS particles (without an MPN coating) revealed the presence of only a few scattered ZIF-8 crystals on the particle surface owing to the weak interaction between PS

and the ZIF-8 precursors (Figure S7). The current study further highlights the essential role of the MPN interface on the formation and growth of crystalline MOF coatings. ZIF-8 coatings with a thickness of ~110 nm were also obtained using smaller PS particles (780 nm) (Figure S8).

The versatility of this MPN-based interfacial strategy was then explored for forming MOFs on diverse particle substrates. For instance, a continuous ZIF-8 coating with a thickness of ~130 nm was successfully grown on MPN-modified melamine formaldehyde particles (Figure 1e, Figure S9a,c,d)—a continuous coating was not possible in the absence of an MPN interface (Figure S9b). Successful ZIF-8 growth on other particle substrates with distinct physicochemical properties across the nanometer-to-micrometer scale includes $CaCO_3$ particles, gold nanoparticles, aminated silica, graphene oxide, and silver nanoparticles. The formation of MPN interlayers and MOF coatings on these substrates was confirmed by their ζ-potential values (Figure 1k)[30] and surface structures (Figure 1f–j, Figure S10f–j). For instance, transmission electron microscopy (TEM) images revealed an increase in the size of the spherical gold nanoparticles from ~50 to ~270 nm upon formation of the MPN@ZIF-8 coatings (Figure 1g, Figure S10d,i).[33] Moreover, crystalline MOF coatings with customized single metals and mixed metals were formed using this strategy, as demonstrated by the presence of Co elements and the corresponding XRD pattern (ascribed to ZIF-67; Figure 1l,m and Figure S11) or Co and Zn elements (ascribed to Co/Zn-ZIF, Figure S12) from EDX mapping results. Compared with other surface modification strategies used for crystalline MOF growth, the MPN-mediated interfacial strategy is facile (e.g., room temperature), rapid (e.g., within seconds), tunable, and can be applied to various substrates (Table S2).

The underlying mechanism of the MPN-based interfacial strategy for the formation of ZIF-67 coatings was investigated by conducting synchrotron X-ray absorption spectroscopy measurements to reveal the coordination geometry of the metal–organic networks at the atomic level. Fourier transform extended X-ray absorption fine structure (FT-EXAFS) spectra of Fe in PS@MPN revealed a dominant peak at ~1.47 Å, which is assigned to the Fe–O bond resulting from the coordination between Fe^{III} and the –OH groups in TA (Figure S13b). This was further evidenced by the distribution in the simultaneous *k*- and *R*-spaces from wavelet transform (WT) analysis (Figure S13c–f). After the growth of a ZIF-67 coating, the coordination number of Fe–O increased from 0.488 to 0.765, which is likely due to the transition of complexation state from bis- to tris-complex (Figure 1n, Figure S14, Figure S16a,b and Table S3), along with the emergence of Co–O and Co–N coordination at 2.48 and 1.41 Å (Figure 1o,p, Figure S15, Figure S16c,d and Table S4). This result indicates that the free –OH groups in MPNs can act as coordination sites to interact with Co^{2+} that further coordinate with organic ligands to form crystalline MOF coatings.

Next, the formation of crystalline MOF coatings on planar substrates was studied. Quartz crystal microbalance (QCM) measurements that were performed in situ while adding MOF precursors showed a significant change in the resonance frequency in the presence of an MPN-modified PS planar electrode, whereas only a slight change in the frequency was observed in the presence of an unmodified electrode (Figure 2a). This further indicated that the MPN interface is essential for the formation of crystalline MOFs on substrates. Successful MPN deposition on a planar glass slide was visualized by a color change from transparent to purple (Figure S17a inset), as well as the appearance of a characteristic TA–Fe ligand-to-metal charge-transfer band in the UV–vis absorption spectra (Figure S17a). After MOF growth and crystallization on the MPN-coated glass, FTIR results showed new peaks at 1145 and 1300 cm^{-1} (C–N vibration), 1581 cm^{-1} (C=N vibration), 2928 and 3134 cm^{-1} (aliphatic and aromatic C–H stretching vibration), which are ascribed to the imidazole ring (Figure S17b).[19,32]

The physicochemical properties of the crystalline MOF films were further tuned and engineered. Atomic force microscopy (AFM) images revealed an initial MPN interfacial layer (~15 nm) on the silicon wafer (Figure 2b), which is consistent with the literature.[30g] Subsequent growth of ZIF-8 on the interfacial layer resulted in a final coating thickness of ~150 nm (Figure 2c), indicating a significantly thicker crystalline MOF coating than the amorphous MPN interfacial layer. EDX mapping images revealed the presence of Zn and N (Figure S18), and the water contact angle (WCA) of the MPN-coated Si wafer changed from 61° to 86° after ZIF-8 coating owing to the relative hydrophobicity of ZIF-8 (Figure S19).[32]

We next investigated the growth of the ZIF-8 film over time (Figure 2d,e and Figure S20). As the reaction proceeded from 20 min to 8 h, the thickness increased from 92 ± 6 to 185 ± 9 nm (Figure 2e). Beyond 8 h, there was no noticeable increase in thickness, likely due to precursor depletion (e.g., 12 and 24 h, Figure 2d, Figure S21a,b). However, further addition of the precursors could reinitiate MOF growth, producing more distinct crystalline shapes (Figure S21c). As observed from Figure S22, the degree of MOF crystallization increased with reaction time. ZIF-8 films formed at 8 h displayed relatively weak diffraction peaks in comparison with those obtained at longer reaction times (e.g., 12 h) or after a secondary growth step (e.g., 8 h + 16 h) that displayed high crystallinity and purity. The thickness and growth kinetics could also be modulated by using different precursor concentrations. Low precursor concentrations typically resulted in discontinuous particles on the substrate surface, whereas higher precursor concentrations led to continuous crystalline films (Figure S23).

Crystalline MOFs were also grown on other planar and tubular substrates, including stainless steel wire mesh of different sizes, polycarbonate (PC), polydimethylsiloxane, Au, and polyfluoroalkoxy (Figure 2f,g and Figures S24–S26). Crystalline MOFs with different metal ions (Zn^{2+} and Co^{2+}), morphologies (e.g., two-dimensional leaf-like ZIF (ZIF-L)),[31b] and subtypes (e.g., UiO-66 and MIL-100) were also grown (Figure 2h,i and Figures S27–S30).

The thin and continuous crystalline MOF coatings obtained via the present MPN-based interfacial strategy represent potential candidates as selective membranes for

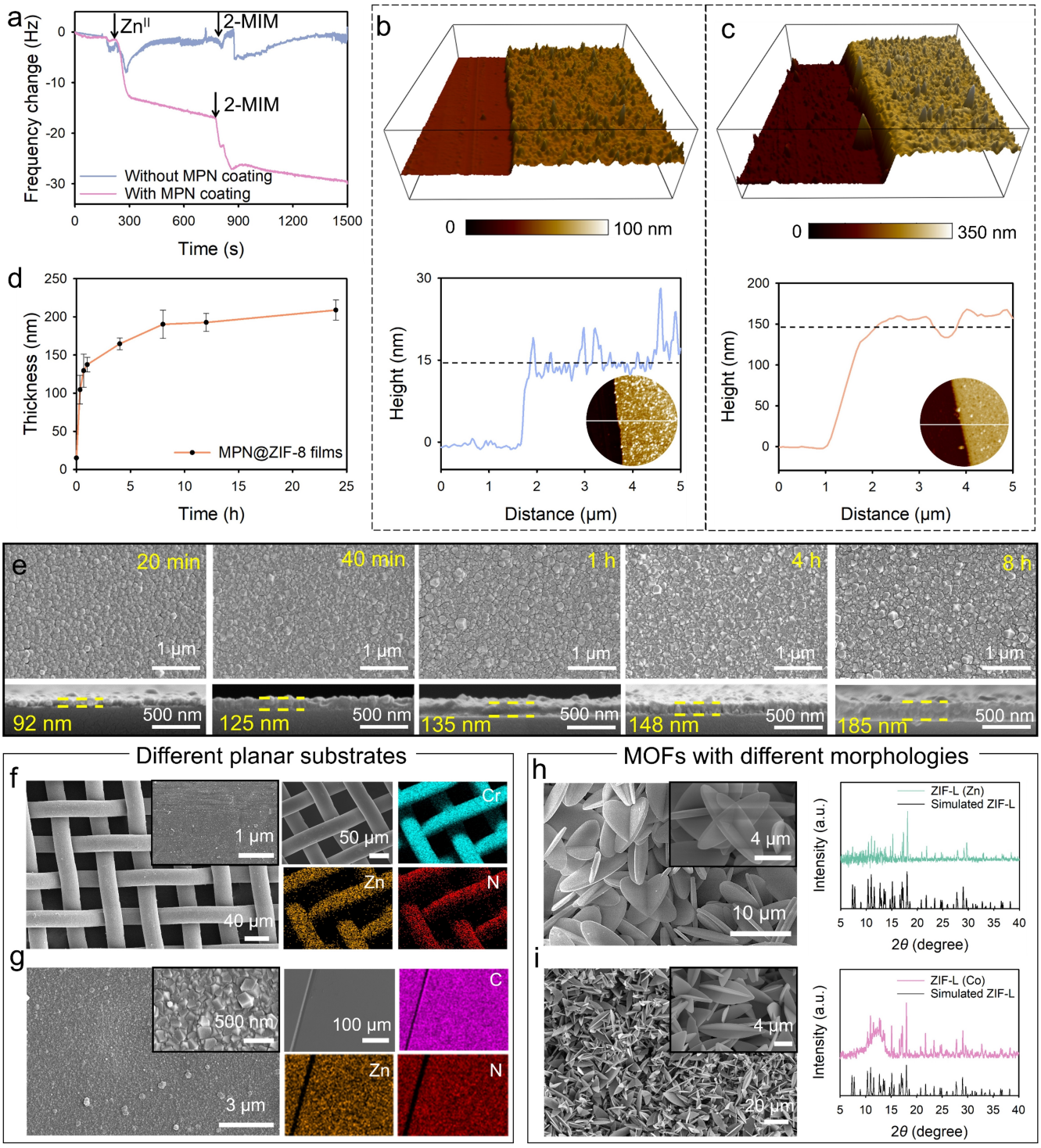

Figure 2. (a) Frequency change of ZIF-8 films on PS-coated QCM electrodes with or without MPN precoating. (b,c) Three-dimensional AFM images, line profiles, and two-dimensional AFM images (insets) of MPN films (b) and MPN@ZIF-8 films (c) on Si wafers. The black regions represent the scratched areas. (d) Thickness of MPN@ZIF-8 films obtained after different reaction times, as measured by AFM. Data are shown as the mean ± standard deviation ($n=3$). (e) SEM images of the surface and cross-section of crystalline MOFs after different reaction times. (f,g) SEM and EDX images of ZIF-8 films grown on MPN-modified stainless steel wire mesh 1 (f) and PC (g). (h,i) SEM images and XRD patterns of ZIF-L (Zn) (h) and ZIF-L (Co) (i) films on MPN-modified Si wafers, and simulated ZIF-L.

liquid and gas separation applications. MPN-coated stainless steel wire mesh 1 was chosen as the substrate for growing crystalline MOFs for immiscible liquid separation (e.g., water–organic solvents). The mesh, which was originally hydrophobic (110°), turned hydrophilic (72°) after MPN deposition but reverted to being more hydrophobic (137°),

though it remained stable in water, after subsequent ZIF-8 coating (Figure 3a). A gravity-driven separation experiment was conducted where a mixture of dichloromethane (DCM, dyed with oil red O) and water (dyed with methylene blue) was passed through the mesh 1@MPN@ZIF-8 membrane—only DCM rapidly permeated through the membrane with a high separation efficiency (99.5 %) and permeate flux of 10574 $L m^{-2} h^{-1}$ (Figure 3b,c and Table S5). Other organic solvents, including chloroform, petroleum ether, hexane, and toluene, were also separated with high efficiency i.e., 99.8 %, 99.6 %, 98.2 %, and 98.3 %, respectively. The reusability of mesh 1@MPN@ZIF-8 as a filter membrane for separating DCM and water was demonstrated by the high separation efficiency (>98 %) and WCA (despite being slightly lower (126°) than the original WCA (137°)) maintained across the 15 cycles studied (Figure S31). MPN-coated PC with pores of 100 nm in size was chosen as a substrate to grow crystalline MOFs for gas separation (Figures S32–S34 and Table S6). The ZIF-8-coated membrane displayed good flexibility as no morphological changes, fragmentation, or detachment of the ZIF-8 coating was observed for the surface or cross-section of the membrane after buckling (Figure 3d,e).[10,11,23,28] The single-gas separation studies (including H_2, CO_2, N_2, CH_4, C_3H_6,

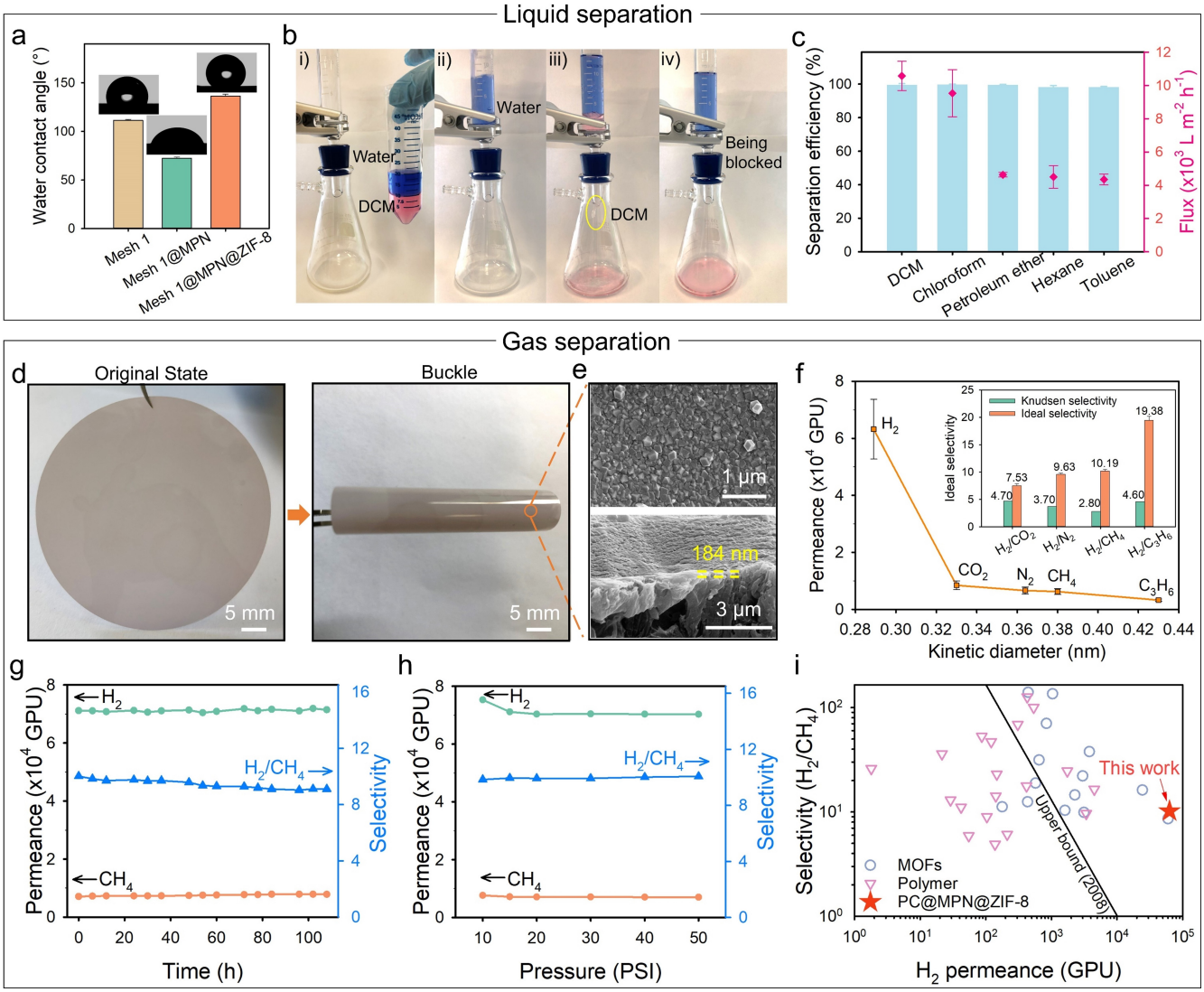

Figure 3. (a) WCA of mesh 1, mesh 1@MPN, and mesh 1@MPN@ZIF-8 in air. The error bars represent standard deviations ($n=3$). (b) Photographs showing the separation of a DCM–water mixture using mesh 1@MPN@ZIF-8 membrane. (c) Separation efficiency of mesh 1@MPN@ZIF-8 membranes for different organic solvents/water mixtures. The error bars represent standard deviations ($n=3$). (d) Photographs showing the flexibility of a PC@MPN@ZIF-8 membrane. (e) Surface and cross-section morphologies of the PC@MPN@ZIF-8 membrane after bending. (f) Single-gas performances of PC@MPN@ZIF-8 membranes at 10 PSI as a function of gas of different kinetic diameters. The inset shows the ideal gas selectivity and Knudsen selectivity. Data are shown as the mean ± standard deviation ($n=3$). (g) Long-term stability of the PC@MPN@ZIF-8 membrane for H_2/CH_4 separation. (h) H_2/CH_4 separation performances of the PC@MPN@ZIF-8 membrane as a function of pressure. (i) Comparison of the H_2/CH_4 separation performance of the PC@MPN@ZIF-8 membrane with literature materials (reference data are provided in Table S8). The "Upper bound (2008)" represents the empirical relationship for membrane separation of gases.[34]

and C_3H_8) revealed that the PC@MPN@ZIF-8 membrane exhibited one of the highest H_2 permeance (63200 GPU) among reported ZIF-8 membranes,[28] likely due to its relatively thin (~180 nm) and nanoscale nature, facilitating faster contact between the feed gas and ZIF-8 crystals (Figure 3f and Table S6).[28,35] Additionally, the superior H_2 permeance exceeded those observed for larger gases owing to the pore sizes and the well-known lattice flexibility of the ZIF-8 nanostructures. Note that the pores of MPN interfacial layers (highly permeable to dextrans with a molecular weight of ~10 kDa) under current synthesis conditions are significantly larger than the size of gas molecules and thus the MPN interfacial layers do not possess gas selectivity properties (Table S6).[30a] The ideal separation selectivity for the PC@MPN@ZIF-8 membranes for H_2/CO_2, H_2/N_2, H_2/CH_4, H_2/C_3H_6, and H_2/C_3H_8 are 7.53, 9.63, 10.19, 19.38, and 43.59 (Figure 3f and Table S6), respectively, surpassing the corresponding Knudsen selectivity (4.70, 3.70, 2.80, 4.60, and 4.69). Moreover, the PC@MPN@ZIF-8 membrane displayed excellent operation stability, as assessed over a 108 h experiment conducted at elevated pressure (Figure 3g,h), effective binary gas separation capacity (Table S7), and promising H_2/CH_4 separation performance with ultrahigh H_2 permeance compared with the separation performance of other reported membranes (Figure 3i, Table S8).

Conclusion

We have demonstrated a facile, versatile, and tunable MOF coating strategy using MPNs as an interfacial layer. This strategy was applied to various crystalline MOF coatings (e.g., ZIF-8, ZIF-67, Co/Zn-ZIF, and ZIF-L) with tailored metal ions and morphologies on various substrates (13 representative types), including particle and planar substrates with different compositions, sizes, and surface chemistries. The thickness and crystalline degrees of the coating were readily tuned by altering the metal-to-ligand ratio and reaction time. Furthermore, the ZIF-8-coated substrates (e.g., stainless steel wire mesh and PC) exhibited exceptional liquid and gas separation performance with an ultrahigh H_2 permeance and good H_2/CH_4 selectivity. This facile and versatile MPN interfacial strategy is promising for engineering crystalline MOF coatings on various substrates for a broad range of applications.

Acknowledgements

This research was funded by the Australian Research Council (ARC) through the Discovery Project (DP240102343) Scheme. F.C. acknowledges the award of a National Health and Medical Research Council Leadership Fellowship (Grant no. GNT2016732). Z.L. acknowledges The University of Melbourne for an Early Career Researcher grant. J.J.R. is the recipient of an ARC Future Fellowship (Project no. FT210100669) funded by the Australian Government. S.P. acknowledges the National Natural Science Foundation of China (Grant no. 22378105 and 23FAA02526). This work was performed in part at the Materials Characterisation and Fabrication Platform (MCFP), Biosciences Microscopy Unit, and the Bio21 Institute at The University of Melbourne. X-ray absorption spectroscopy experiments were conducted at the Australian Synchrotron, part of ANSTO (Grant No. 18766). We acknowledge Dr. Marco Cassani, Dr. Shiyao Li, Dr. Christina Cortez-Jugo, and Dr. Yi Ju for their helpful discussions. Open Access publishing facilitated by The University of Melbourne, as part of the Wiley - The University of Melbourne agreement via the Council of Australian University Librarians.

Conflict of Interest

The authors declare no conflict of interest.

Data Availability Statement

The data that support the findings of this study are available from the corresponding author upon reasonable request.

Keywords: metal–organic frameworks · metal–phenolic networks · separation membranes · surface chemistry · thin films

[1] H. Furukawa, K. E. Cordova, M. O'Keeffe, O. M. Yaghi, *Science* **2013**, *341*, 1230444.
[2] Z. Lin, J. J. Richardson, J. Zhou, F. Caruso, *Nat. Chem. Rev.* **2023**, *7*, 273–286.
[3] S. M. Moosavi, A. Nandy, K. M. Jablonka, D. Ongari, J. P. Janet, P. G. Boyd, Y. Lee, B. Smit, H. J. Kulik, *Nat. Commun.* **2020**, *11*, 4068.
[4] a) J. Meng, X. Liu, C. Niu, Q. Pang, J. Li, F. Liu, Z. Liu, L. Mai, *Chem. Soc. Rev.* **2020**, *49*, 3142–3186; b) X. Peng, X. Wu, M. Zhang, H. Yuan, *ACS Sens.* **2023**, *8*, 2471–2492.
[5] A. Bavykina, N. Kolobov, I. S. Khan, J. A. Bau, A. Ramirez, J. Gascon, *Chem. Rev.* **2020**, *120*, 8468–8535.
[6] G. Lu, S. Li, Z. Guo, O. K. Farha, B. G. Hauser, X. Qi, Y. Wang, X. Wang, S. Han, X. Liu, J. S. DuChene, H. Zhang, Q. Zhang, X. Chen, J. Ma, S. C. Loo, W. D. Wei, Y. Yang, J. T. Hupp, F. Huo, *Nat. Chem.* **2012**, *4*, 310–316.
[7] K. Liang, R. Ricco, C. M. Doherty, M. J. Styles, S. Bell, N. Kirby, S. Mudie, D. Haylock, A. J. Hill, C. J. Doonan, P. Falcaro, *Nat. Commun.* **2015**, *6*, 7240.
[8] H. Zheng, Y. Zhang, L. Liu, W. Wan, P. Guo, A. M. Nystrom, X. Zou, *J. Am. Chem. Soc.* **2016**, *138*, 962–968.
[9] K. Liang, J. J. Richardson, C. J. Doonan, X. Mulet, Y. Ju, J. Cui, F. Caruso, P. Falcaro, *Angew. Chem. Int. Ed.* **2017**, *56*, 8510–8515.
[10] G. Liu, V. Chernikova, Y. Liu, K. Zhang, Y. Belmabkhout, O. Shekhah, C. Zhang, S. Yi, M. Eddaoudi, W. J. Koros, *Nat. Mater.* **2018**, *17*, 283–289.
[11] a) L. H. Xu, S. H. Li, H. Mao, Y. Li, A. Zhang, S. Wang, W. M. Liu, J. Lv, T. Wang, W. W. Cai, L. Sang, W. W. Xie, C. Pei, Z. Z. Li, Y. N. Feng, Z. P. Zhao, *Science* **2022**, *378*, 308–312; b) H. Yuan, K. Li, D. Shi, H. Yang, X. Yu, W. Fan, P. J. S. Buenconsejo, D. Zhao, *Adv. Mater.* **2023**, *35*, 2211859.
[12] G. Chen, C. Chen, Y. Guo, Z. Chu, Y. Pan, G. Liu, G. Liu, Y. Han, W. Jin, N. Xu, *Science* **2023**, *381*, 1350–1356.

[13] Q. Liu, Y. Miao, L. F. Villalobos, S. Li, H. Y. Chi, C. Chen, M. T. Vahdat, S. Song, D. J. Babu, J. Hao, Y. Han, M. Tsapatsis, K. V. Agrawal, *Nat. Mater.* **2023**, *22*, 1387–1393.
[14] H. Bux, F. Liang, Y. Li, J. Cravillon, M. Wiebcke, J. Caro, *J. Am. Chem. Soc.* **2009**, *131*, 16000–16001.
[15] S. R. Venna, M. A. Carreon, *J. Am. Chem. Soc.* **2010**, *132*, 76–78.
[16] X. J. Bai, X. Y. Lu, R. Ju, H. Chen, L. Shao, X. Zhai, Y. N. Li, F. Q. Fan, Y. Fu, W. Qi, *Angew. Chem. Int. Ed.* **2021**, *60*, 701–705.
[17] H. T. Kwon, H. K. Jeong, *J. Am. Chem. Soc.* **2013**, *135*, 10763–10768.
[18] A. J. Brown, N. A. Brunelli, K. Eum, F. Rashidi, J. R. Johnson, W. J. Koros, C. W. Jones, S. Nair, *Science* **2014**, *345*, 6192.
[19] W. Li, P. Su, Z. Li, Z. Xu, F. Wang, H. Ou, J. Zhang, G. Zhang, E. Zeng, *Nat. Commun.* **2017**, *8*, 406.
[20] I. Stassen, M. Styles, G. Grenci, H. V. Gorp, W. Vanderlinden, S. D. Feyter, P. Falcaro, D. D. Vos, P. Vereecken, R. Ameloot, *Nat. Mater.* **2016**, *15*, 304–310.
[21] X. Ma, P. Kumar, N. Mittal, A. Khlyustova, P. Daoutidis, K. A. Mkhoyan, M. Tsapatsis, *Science* **2018**, *361*, 1008–1011.
[22] S. Zhou, Y. Wei, L. Li, Y. Duan, Q. Hou, L. Zhang, L. Ding, J. Xue, H. Wang, J. Caro, *Sci. Adv.* **2018**, *4*, eaau1393.
[23] Y. Zhao, Y. Wei, L. Lyu, Q. Hou, J. Caro, H. Wang, *J. Am. Chem. Soc.* **2020**, *142*, 20915–20919.
[24] a) B. Y. Guan, L. Yu, X. W. D. Lou, *Adv. Sci.* **2017**, *4*, 1700247; b) M. S. Alivand, O. Mazaheri, Y. Wu, A. Zavabeti, A. J. Christofferson, N. Meftahi, S. P. Russo, G. W. Stevens, C. A. Scholes, K. A. Mumford, *Nat. Commun.* **2022**, *13*, 1249; c) H. Yuan, J. Cui, N. Li, M. Li, X. Yu, W. Fan, A. Karmakar, J. Dong, S. J. Pennycook, H. Cai, D. Zhao, *ACS Appl. Mater. Interfaces* **2020**, *12*, 36715–36722.
[25] R. Xu, Y. Kang, W. Zhang, X. Zhang, B. Pan, *Angew. Chem. Int. Ed.* **2022**, *61*, e202115443.
[26] E. Barankova, X. Tan, L. F. Villalobos, E. Litwiller, K. V. Peinemann, *Angew. Chem. Int. Ed.* **2017**, *56*, 2965–2968.
[27] a) Q. Liu, N. Wang, J. Caro, A. Huang, *J. Am. Chem. Soc.* **2013**, *135*, 17679–17682; b) J. Zhou, P. Wang, C. Wang, Y. T. Goh, Z. Fang, P. B. Messersmith, H. Duan, *ACS Nano* **2015**, *9*, 6951–6960.
[28] J. Hou, P. D. Sutrisna, Y. Zhang, V. Chen, *Angew. Chem. Int. Ed.* **2016**, *55*, 3947–3951.
[29] a) J. Zhou, Z. Lin, Y. Ju, M. A. Rahim, J. J. Richardson, F. Caruso, *Acc. Chem. Res.* **2020**, *53*, 1269–1278; b) D. Wu, J. Zhou, M. N. Creyer, W. Yim, Z. Chen, P. B. Messersmith, J. V. Jokerst, *Chem. Soc. Rev.* **2021**, *50*, 4432–4483; c) H. Geng, Q. Z. Zhong, J. Li, Z. Lin, J. Cui, F. Caruso, J. Hao, *Chem. Rev.* **2022**, *122*, 11432–11473.
[30] a) H. Ejima, J. J. Richardson, K. Liang, J. P. Best, M. P. van Koeverden, G. K. Such, J. Cui, F. Caruso, *Science* **2013**, *341*, 154–157; b) Z. Lin, J. Zhou, C. Cortez-Jugo, Y. Han, Y. Ma, S. Pan, E. Hanssen, J. J. Richardson, F. Caruso, *J. Am. Chem. Soc.* **2020**, *142*, 335–341; c) Z. Lin, J. Zhou, Y. Qu, S. Pan, Y. Han, R. P. M. Lafleur, J. Chen, C. Cortez-Jugo, J. J. Richardson, F. Caruso, *Angew. Chem. Int. Ed.* **2021**, *60*, 24968–24975; d) S. Pan, E. Goudeli, J. Chen, Z. Lin, Q. Z. Zhong, W. Zhang, H. Yu, R. Guo, J. J. Richardson, F. Caruso, *Angew. Chem. Int. Ed.* **2021**, *60*, 14586–14594; e) J. Guo, B. L. Tardy, A. J. Christofferson, Y. Dai, J. J. Richardson, W. Zhu, M. Hu, Y. Ju, J. Cui, R. R. Dagastine, I. Yarovsky, F. Caruso, *Nat. Nanotechnol.* **2016**, *11*, 1105–1111; f) X. Yang, Y. Li, D. Wu, L. Yan, J. Guan, Y. Wen, Y. Bai, B. B. Mamba, S. B. Darling, L. Shao, *Proc. Natl. Acad. Sci. USA* **2024**, *121*, e2319390121; g) G. Yun, D. G. Kang, H. B. Rheem, H. Lee, S. Y. Han, J. Park, W. K. Cho, S. M. Han, I. S. Choi, *Langmuir* **2020**, *36*, 15552–15557.
[31] a) K. S. Park, Z. Ni, A. P. Cote', J. Y. Choi, R. Huang, F. J. Uribe-Romo, H. K. Chae, M. O'Keeffe, O. M. Yaghi, *Proc. Natl. Acad. Sci. USA* **2006**, *103*, 10186–10191; b) A. Deacon, L. Briquet, M. Malankowska, F. Massingberd-Mundy, S. Rudić, T. L. Hyde, H. Cavaye, J. Coronas, S. Poulston, T. Johnson, *Commun. Chem.* **2022**, *5*, 18.
[32] W. Liang, H. Xu, F. Carraro, N. K. Maddigan, Q. Li, S. G. Bell, D. M. Huang, A. Tarzia, M. B. Solomon, H. Amenitsch, L. Vaccari, C. J. Sumby, P. Falcaro, C. J. Doonan, *J. Am. Chem. Soc.* **2019**, *141*, 2348–2355.
[33] J. Zhou, M. Penna, Z. Lin, Y. Han, R. P. M. Lafleur, Y. Qu, J. J. Richardson, I. Yarovsky, J. V. Jokerst, F. Caruso, *Angew. Chem. Int. Ed.* **2021**, *60*, 20225–20230.
[34] L. M. Robeson, *J. Membr. Sci.* **2008**, *320*, 390–400.
[35] M. Kanezashi, K. Yada, T. Yoshioka, T. Tsuru, *J. Am. Chem. Soc.* **2009**, *131*, 414.

Manuscript received: May 28, 2024
Accepted manuscript online: June 23, 2024
Version of record online: ■■, ■■

Research Article

MOF Membranes

T. Wang, Z. Lin, O. Mazaheri, J. Chen, W. Xu, S. Pan, C.-J. Kim, J. Zhou, J. J. Richardson, F. Caruso* _ **e202410043**

Crystalline Metal–Organic Framework Coatings Engineered via Metal–Phenolic Network Interfaces

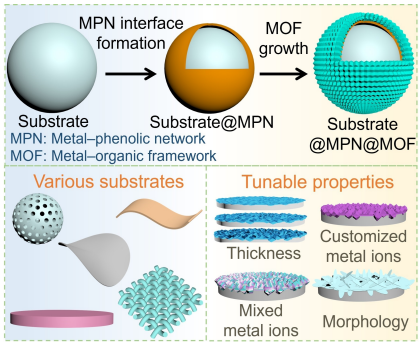

A metal–phenolic network interfacial strategy is developed to form crystalline metal–organic frameworks (MOFs) on diverse particle and planar substrates. This strategy allows for customized physicochemical properties (e.g., thickness, and morphology) of the supported crystalline MOFs, with potential for biomedical, agricultural, and energy applications.